Chemical Engineering Science 252 (2022) 117284

Contents lists available at ScienceDirect

Chemical Engineering Science

journal homepage: www.elsevier.com/locate/ces

Theoretical calculations and CFD simulations of membrane reactor designs

Hong Huang [a,*], Remzi Can Samsun [a], Ralf Peters [a], Detlef Stolten [b,c,d]

[a] Electrochemical Process Engineering (IEK-14), Forschungszentrum Jülich GmbH, Jülich 52425, Germany
[b] Techno-Economic Systems Analysis (IEK-3), Forschungszentrum Jülich GmbH, Jülich 52425, Germany
[c] JARA-ENERGY, Aachen 52056, Germany
[d] Chair for Fuel Cells, RWTH Aachen University, Aachen 52072, Germany

HIGHLIGHTS

- Building of the relationship of equilibrium constant-conversion-*DaPe* for membrane reactors in a general form.
- Exemplification of the relationship by the dry reforming of methane and reverse water gas shift by theoretical calculations.
- Analysis of the compatibility of reaction kinetics with membrane permeation flux and the effects of reactor geometry by CFD simulations.
- Identification and highlight of the contribution of stoichiometric coefficient to conversion enhancement.

GRAPHICAL ABSTRACT

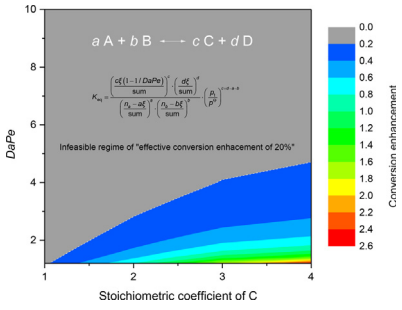

ARTICLE INFO

Article history:
Received 24 June 2021
Received in revised form 2 November 2021
Accepted 15 November 2021
Available online 19 November 2021

Keywords:
Membrane reactor
Damköhler number
Péclet number
Stoichiometric coefficient
Compatibility

ABSTRACT

Membrane reactors are promising for enabling various reactions that are thermodynamically-limited. Yet research into their design is often performed on a case-by-case basis; also, no general but quantified analysis has been conducted on the selection and matching of suitable membranes for reactions. In this study, we first introduce two dimensionless numbers, – namely the Damköhler (*Da*) and Péclet (*Pe*) numbers. We then develop the relationship of equilibrium constant-conversion-*DaPe* in a general form for membrane reactors, which incorporates the parameters of the operating conditions and reaction stoichiometric coefficients. To exemplify the relationship, it is applied to the reactions of the dry reforming of methane and reverse water gas shift using theoretical calculations. Subsequently, an analysis of the compatibility of the reaction kinetics and permeation flux, as well as the effects of reactor geometry characteristics is performed by means of CFD simulations. Finally, we discuss the relationship of the stoichiometric coefficient and conversion enhancement. Beyond the contribution to conversion enhancement by the operating conditions, it is informed that the contribution of the stoichiometric coefficient should also be effectively leveraged in order to achieve higher conversion enhancement, especially for reactions that feature higher equilibrium constants. The relationships derived in this study deliver insights into the selection and matching of membranes for a given reaction prior to detailed designs being developed.

* Corresponding author.
E-mail address: h.huang@fz-juelich.de (H. Huang).

https://doi.org/10.1016/j.ces.2021.117284
0009-2509/

Nomenclature

c_i	species concentration (mol m^{-3})
Da	Damköhler number
D_{ij}	binary diffusion coefficient (m^2/s)
$D_{T,i}$	thermal diffusion coefficient (m^2/s)
E_{H_2}	activation energy of the palladium membrane (J mol^{-1})
F_{tot}	flowrate of reactants (mol s^{-1})
J_i	diffusive flux (kg m^{-2} s^{-1})
n_{H_2}	moles of H_2 (mol)
n_{CO_2}	moles of CO_2 (mol)
k_1, k_2, k_3	pre-exponential factor of the reactions (mol kg^{-1} s^{-1})
k_{H_2}	pre-exponential factor of the palladium membrane (mol m^{-2} s^{-1} Pa^{-1})
K_{eq}	equilibrium constant
Pe	Péclet number
p_i	partial pressure of species (Pa)
p_t	total pressure (Pa)
Q_{H_2O}	permeance of the zeolite membrane (mol m^{-2} s^{-1} Pa^{-1})
r	reaction rate, (mol kg^{-3} s^{-1})
S	source term
v	velocity (m s^{-1})
W_{cat}	catalyst weight (kg)
X_i	conversion of species
y_i	mole fraction of species
Y_i	mass fraction of species
$K_{CO_2}1$, $K_{CO_2}2$, K_{CH_4}, K_{H_2}	adsorption constant
ΔXi	conversion enhancement

Greek letters

ξ	reaction extent
η_o	overall effectiveness factor
ρ	density (kg m^{-3})

1. Introduction

Membrane reactors have many possible applications, and of the many factors that suggest their use, boosting conversion is one of the major goals for chemical reactions with thermodynamic limitations, and is achieved by leveraging Le Chatelier's principle. Previous studies have focused on the membrane reactor applications of different reactions. Reforming reactions (i.e., the steam reforming of methane/methanol), shift reactions ((reverse) water gas shift) and fuel synthesis reactions (methanol, Fischer-Tropsch synthesis) are often used as case studies. The methodologies used in these studies include experimental (Fabián-Anguiano et al., 2019); (Wade et al., 2011), numerical simulation (Sommer and Kirchen, 2019); (Yang et al., 2019) and techno-economic analyses (Kim et al., 2018); (Kim et al., 2019). These studies have clearly shown the potential of membrane reactors, yet most of the studies were performed in a case-by-case manner, with a small number focusing on the selection and analysis of membrane reactors in a general manner. In addition, these investigations have been carried out under different conditions, which makes it difficult to conduct like-for-like comparisons across different reactions.

In addition, as different membrane types become increasingly available, another question arises: which kind of membrane should be matched for a reaction and to what extent can the membrane enhance the reaction during conversion? This problem occurs in many reaction systems where more than one product can be removed by membranes. This is especially the case when hydrogen and carbon dioxide are both present in products. For simple reactions such as water gas shift (one reaction), hydrogen permeable membranes may be preferentially used to enhance the conversion, which is plausible because removing any one of the products (hydrogen or carbon dioxide) can achieve the same gains in conversion. For more complex reaction systems such as the steam reforming of methane (three reactions), using a preconceived membrane such as a palladium membrane is problematic, as its performance is not quantified before such a choice is made. For example, (Wu et al., 2020) evaluated a CO_2-permselective membrane reactor rather than a hydrogen-permeable membrane for the steam reforming of methane. It was shown that the membrane reactor could achieve a high hydrogen yield of 90% with 84% CO_2 recovery. Yet if a hydrogen permeable membrane is used in the same reaction; many studies have reported hydrogen recovery of around 80% without CO_2 recovery (Iulianelli et al., 2010); (Patrascu and Sheintuch, 2015). These results suggest that hydrogen-permeable membranes do not necessarily perform better than CO_2 ones for a given reaction. Another example is the methanol synthesis from CO_2 and H_2 in membrane reactors. Many studies have used water-permeable membranes to enhance the conversion (Gallucci and Basile, 2007); (Gallucci et al., 2004); (Raso et al., 2021). In fact, methanol-permeable (zeolite) membranes are also available and applicable for this reaction, but have received little attention. A study by (Barbieri et al., 2002) revealed that a membrane reactor with CH_3OH removal can lead to higher selectivity and yields compared to the oft-used water-permeable membrane reactors. All of these examples reflect the common problem that the selection and matching of membranes for a reaction cannot be simply based on qualitative analysis and judgement. While the determination of a suitable membrane for a reaction is subject to many factors, such as membrane flux, selectivity, stability, and cost, research and development often begins before these specific parameters are known.

Addressing the question of how to select and match membranes for a reaction requires a general and quantified analysis that is reaction-independent, and thus widely applicable. In this study, we first introduce a dimensionless number group consisting of the Péclet and Damköhler numbers – *DaPe* – and then outline the relationship of equilibrium constant-conversion-*DaPe*. This relationship is exemplified by some representative reactions of the dry reforming of methane (DRM) and reverse water gas shift (RWGS) via theoretical calculations. The compatibility of membranes with reactions from the perspectives of reaction kinetics-permeation flux and reactor geometric characteristics is then analysed by means of computational fluid dynamics (CFD) simulations. Finally, we discuss the relationship between *DaPe* and the stoichiometric coefficient to investigate the latter to conversion enhancement and the implications for membrane reactor selection. These relationships can be easily applied to reactions of one's own interest without expending much effort.

2. Theoretical calculations

In this section, we will first build the relationship of equilibrium constant-conversion-*DaPe*. To validate this, it is then applied to the reactions of DRM and RWGS.

2.1. Relationship of equilibrium constant-conversion-DaPe

We begin the analysis with a single chemical reaction in a general form:

$$a\ A\ + b\ B\ \leftrightarrow c\ C\ + d\ D \tag{1}$$

where a, b, c, and d are the stoichiometric coefficients of each species. In reality, many reaction systems involve multiple reactions, but this would needlessly complicate the calculations. If the reaction is in the equilibrium state, the relationship between the equilibrium constant and partial pressure or molar fraction of each species is well-recognized and is given by the following:

$$K_{eq} = \frac{\left(\frac{p_C}{p^\Theta}\right)^c \cdot \left(\frac{p_D}{p^\Theta}\right)^d}{\left(\frac{p_A}{p^\Theta}\right)^a \cdot \left(\frac{p_B}{p^\Theta}\right)^b} = \frac{y_C^c \cdot y_D^d}{y_A^a \cdot y_B^b} \cdot \left(\frac{p_t}{p^\Theta}\right)^{c+d-a-b} \tag{2}$$

where K_{eq} is the equilibrium constant, p_i is the partial pressure, y_i is the mole fraction, p_t is total pressure, and p^Θ is the standard pressure of 1 bar. Here, we have implicitly used the assumption that the reaction is in the gas phase, and one can easily replace pressure with activity in Eq. (2) for liquid phase reactions. If the operating conditions (T and p_t) and initial compositions are given, we can calculate the equilibrium molar fractions of all species.

Now consider this reaction taking place in a membrane reactor and that one of the species is to be removed by membrane permeation (C or D). In order to build the relationship between K_{eq} and y_i for membrane reactors, we first introduce two dimensionless numbers: the Damköhler number (*Da*) and the Péclet one (*Pe*). The Damköhler number is defined as the ratio of the reaction rates to the flowrates of reactants and the Péclet number is the ratio of the flowrates of reactants to the membrane permeation fluxes according to (Bernstein and Lund, 1993); (Moon and Park, 2000); and (Dixon, 2001):

$$Da = \frac{r_i \cdot W_{cat}}{F_{tot}} \tag{3}$$

$$Pe = \frac{F_{tot}}{J_i} \tag{4}$$

where r_i is the reaction rate, W_{cat} is the catalyst weight, F_{tot} is the flowrate of reactants, and J_i is the membrane flux. Since the reaction rate is based on the catalyst weight, it has to be assumed that the catalyst is well dispersed and active all over its mass. Drawing on these two numbers, we can further derive a dimensionless number group – *DaPe* – that is the product of the two numbers:

$$DaPe = \frac{r_i \cdot W_{cat}}{J_i} \tag{5}$$

DaPe represents the ratio of the reaction rate to the membrane permeation rate, which is a very useful indicator to evaluate the relative magnitude of the reaction and membrane permeation rates. A high *DaPe* indicates that the reaction is much faster than membrane permeation, whereas a low one means that membrane permeation is faster than the reaction. Mathematically, the lower limit of *DaPe* is unity if no product is fed with reactants, as the membrane permeation rates cannot exceed the reaction rates. The reciprocal of *DaPe* – $1/DaPe$ has a clear physical meaning: the percentage of species removed by membrane permeation. (Oyama and Lim, 2009) referred to $1/DaPe$ as operability level coefficient (OLC) and employed this to analyze some reforming reactions, finding that the values of OLC ranging from 0.03 to 0.78 could lead to obvious conversion enhancement.

Next, we will relate *DaPe* to K_{eq} and y_i. Before commencing the relating procedure, the species that is to be removed should be determined, and here we designate C as the target species; note that this designation is without tendency, and any other species on the product side can also be selected. The relating is performed using a stoichiometric table, which provides a functional form that clearly shows the species molar changes before and after the reaction. For this reason, it finds wide use in chemical equilibrium calculations (Al-Megren et al., 2013); (Rezai and Traa, 2008). Assuming that the initial moles of A, B, C, and D are n_a, n_b, 0, and 0, and the reaction extent is ξ, then the equilibrium molar faction can be obtained, as is shown in Table 1.

Using this table, the relationship between the equilibrium constant K_{eq} and *DaPe* for membrane reactors can be derived:

$$K_{eq} = \frac{\left(\frac{c\xi(1-1/DaPe)}{\text{sum}}\right)^c \cdot \left(\frac{d\xi}{\text{sum}}\right)^d}{\left(\frac{n_a - a\xi}{\text{sum}}\right)^a \cdot \left(\frac{n_b - b\xi}{\text{sum}}\right)^b} \cdot \left(\frac{p_t}{p^\Theta}\right)^{c+d-a-b} \tag{6}$$

The *DaPe* variable has been included in Eq. (6). This relationship can be used to study the effects of operating conditions and feed composition with different *DaPe* values. Specially, when the *DaPe* is infinitely large, it is equivalent to a fixed-bed model.

The simplest case described by Eq. (6) is $a = b = c = d = 1$. Fig. 1 depicts this scenario for $K_{eq} = 1$. The purpose of this simplest case is to observe the qualitative trend of conversion of reactants with *DaPe*. It can be seen that the conversion of A or B decreases with *DaPe*, as a higher *DaPe* means less product of C is removed and the conversion is therefore lower, but always higher than the asymptotic value of 0.5. It can also be seen that the changing rate of the conversion becomes much slower when *DaPe* is larger than 3, telling us the removal of C should be larger than a threshold value to achieve meaningful conversion enhancement.

2.2. Applications to DRM and RWGS

To further exemplify the above relationship, we will apply the relationship specified in Eq. (6) to some representative reactions i.e. the DRM and RWGS. As the DRM also comprises a side reaction of RWGS, in order to avoid a potential confusion, the RWGS alone is also referred to as an independent RWGS to stress the difference between the two reactions:

$$CO_2\ +\ CH_4\ \leftrightarrow\ 2CO\ +\ 2H_2 \tag{7}$$

$$CO_2\ +\ H_2\ \leftrightarrow\ CO\ +\ H_2O \tag{8}$$

The expansion of Eq. (6) can be written as below:

$$0 = K_{eq1} - \frac{\left(\frac{(2\xi_1-\xi_2)\cdot(1-1/DaPe)}{1+n_{CO_2}+2\xi_1-(2\xi_1-\xi_2)/DaPe}\right)^2 \cdot \left(\frac{2\xi_1+\xi_2}{1+n_{CO_2}+2\xi_1-(2\xi_1-\xi_2)/DaPe}\right)^2}{\left(\frac{1-\xi_1}{1+n_{CO_2}+2\xi_1-(2\xi_1-\xi_2)/DaPe}\right) \cdot \left(\frac{n_{CO_2}-\xi_1-\xi_2}{1+n_{CO_2}+2\xi_1-(2\xi_1-\xi_2)/DaPe}\right)} \cdot \left(\frac{p_t}{p^\Theta}\right)^2 \tag{9}$$

$$0 = K_{eq2} - \frac{\left(\frac{2\xi_1+\xi_2}{1+n_{CO_2}+2\xi_1-(2\xi_1-\xi_2)/DaPe}\right) \cdot \left(\frac{\xi_2}{1+n_{CO_2}+2\xi_1-(2\xi_1-\xi_2)/DaPe}\right)}{\left(\frac{(2\xi_1-\xi_2)\cdot(1-1/DaPe)}{1+n_{CO_2}+2\xi_1-(2\xi_1-\xi_2)/DaPe}\right) \cdot \left(\frac{n_{CO_2}-\xi_1-\xi_2}{1+n_{CO_2}+2\xi_1-(2\xi_1-\xi_2)/DaPe}\right)} \tag{10}$$

The above is a set of nonlinear equations with two unknowns of ξ_1 and ξ_2, where ξ_1 is the reaction extent of Eq. (7), and ξ_2 the reaction extent of Eq. (8). They can be solved when K_{eq1} and K_{eq2} are specified.

Proceeding in a similar fashion for the independent RWGS, it can be readily shown that:

$$0 = K_{eq3} - \frac{\left(\frac{\xi_3(1-1/DaPe)}{1+n_{H_2}-\xi_3/DaPe}\right) \cdot \left(\frac{\xi_3}{1+n_{H_2}-\xi_3/DaPe}\right)}{\left(\frac{1-\xi_3}{1+n_{H_2}-\xi_3/DaPe}\right) \cdot \left(\frac{n_{H_2}-\xi_3}{1+n_{H_2}-\xi_3/DaPe}\right)} \tag{11}$$

Table 1
Stoichiometric table for the calculation of mole balances of Eq. (1) in membrane reactors.

	A	B	C	D	Total moles
Initial moles	n_a	n_b	0	0	$n_a + n_b$
Moles reacted	$-a\xi$	$-b\xi$	$c\xi(1-1/DaPe)$	$d\xi$	$c\xi(1-1/DaPe) + d\xi - a\xi - b\xi$
Equilibrium moles	$n_a-a\xi$	$n_b-b\xi$	$c\xi(1-1/DaPe)$	$d\xi$	$n_a + n_b + c\xi\cdot(1-1/DaPe) + d\xi - a\xi - b\xi$ = sum
Molar fraction	$\frac{n_a-a\xi}{\text{sum}}$	$\frac{n_b-b\xi}{\text{sum}}$	$\frac{c\xi(1-1/DaPe)}{\text{sum}}$	$\frac{d\xi}{\text{sum}}$	

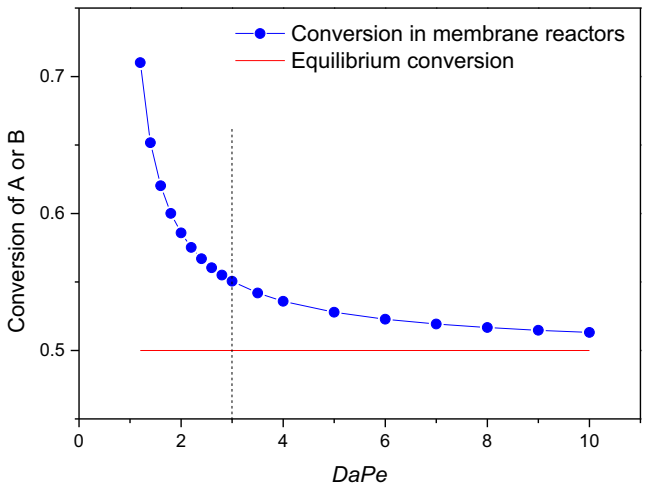

Fig. 1. Conversion of A or B at different *DaPe* by Eq. (6), $a = b = c = d = 1$, $K_{eq} = 1$, $n_a = n_b = 1$.

In Eqs. (9–11), the conversions of CH_4 and CO_2 cannot be directly obtained, and therefore we must still define the conversions and the conversion enhancement according to the reaction extents, as follows:

$$X_{CH_4,\,DRM} = \xi_1 \tag{12}$$

$$X_{CO_2,DRM} = \frac{\xi_1 + \xi_2}{n_{CO_2}} \tag{13}$$

$$X_{CO_2,RWGS} = \xi_3 \tag{14}$$

$$X_{H_2,\,RWGS} = \frac{\xi_3}{n_{H_2}} \tag{15}$$

$$\Delta X_i = \frac{X_{i,m} - X_{i,eq}}{X_{i,eq}} \tag{16}$$

In Eqs. (12)–(15), X represents conversion in the membrane reactors. In Eq. (16), $X_{i,m}$ and $X_{i,eq}$ represent conversions in the membrane reactor and equilibrium conversions and ΔX represents conversion enhancement. Solving Eqs. (9)–(11) yields the conversions of each reaction.

With the relationship and indicators, we will next study how operating conditions affect conversions and their enhancement by using membrane reactors.

We start our analysis of the DRM assuming the following conditions: $T = 600$ ℃, $P = 20$ bar, CH_4:CO_2 = 1:1. These are typical for the reaction and suitable for membrane permeation. In Fig. 2 (a), both the CO_2 and CH_4 conversions monotonically decrease with *DaPe* as the contribution of membranes vanishes due to the decreasing H_2 removal. At a low *DaPe* of 1.2 (83.3% H_2 removal), the CO_2 conversion is 26.8% and CH_4 conversion is 23.0%. However, achieving such a low *DaPe* is not easy and requires high-flux membranes. At a moderate *DaPe* of 2, CO_2 has a conversion of 22.6%, and the CH_4 conversion is 14.6%. It can also be seen that when the *DaPe* is larger than 3, CO_2 conversion is nearly unchanged, but CH_4 conversion still decreases, although at an ever lower rate. As a result, the gap between the conversions becomes ever more significant, suggesting that the removal H_2 has a stronger impact on the CH_4 conversion. The conversion enhancement shown in Fig. 2 (a) also confirms this point. CH_4 conversion enhancement is varied between 101% and 3.4%, whereas that of CO_2 is changed from 22% to 0.25% over the entire range of *DaPe*. Yet the enhancement does not decrease linearly with *DaPe*; instead rapidly at first and then more slowly. In particular, the conversion enhancement of CH_4 is nearly five times that of CO_2 at a *DaPe* of 1.2. Removing H_2 shifts the equilibrium of Eq. (7) to the right side, whereby the CH_4 conversion is increased. However, H_2 is one of the reactants in Eq. (8), and its removal increases CO_2 conversion in the first reaction but suppresses its conversion in the second. The overall result is that CO_2 conversion is increased, but to a limited degree. If we set 20% as the "effective enhancement" threshold for CH_4, then according to Fig. 2 (a), the *DaPe* should be lower than 2.4, which is realizable for most membranes over a wide range of conditions.

The impacts of temperature on CO_2 and CH_4 conversions and the conversion enhancement are depicted in Fig. 2 (b). As expected, raising the temperature to 650 ℃ increases CO_2 and CH_4 conversions as both reactions are endothermic. However, the trend of both with *DaPe* is very similar to that at $T = 600$ ℃, as is the trend of conversion enhancement. In addition, the gap between the two conversions becomes smaller, as the two reactions respond differently to temperature: the equilibrium constant of Eq. (7) is increased from 0.197 to 1.368, whereas that of Eq. (8) rises from 0.366 to 0.481.

Reducing the pressure from 20 to 1 bar can significantly increase both the CO_2 and CH_4 conversions, as is shown in Fig. 2 (c). At *DaPe* = 1.2, the conversions of CO_2 and CH_4 are very close, at 69.8% and 68.1%, respectively. Furthermore, the gap between the two conversions becomes much smaller compared to that at 20 bar. For the conversion enhancement, it is apparent that the CH_4 conversion enhancement is lower (from 66% to 3.4%) but the CO_2 conversion enhancement is higher (from 30.6% to 0.81%). Similar to the effects of temperature, reducing the pressure has stronger influence in Eq. (7). Eq. (8) is an equimolar reaction, and therefore the pressure does not change its equilibria. From a practical perspective, reducing the operating pressure is not good for membrane permeation, as it is a source of the driving force of membrane permeation. In reality, the operating pressure is a factor that must be balanced between conversion and permeation.

Neither temperature nor pressure leads to a CH_4 conversion higher than the CO_2 conversion, even with a low *DaPe*. Instead, changing the feed composition is an effective way achieving this effect. When CH_4:CO_2 = 1:2, the equilibrium conversions of CO_2 and CH_4 are nearly the same (17.9% and 17.4%); combined with the contribution of *DaPe*, the CH_4 conversion (33.2%) can be much higher than the CO_2 one (20.5%), as is displayed in Fig. 2 (d). Unlike the conversion gaps depicted in Fig. 2 (a) to (c), the gap between the conversions becomes ever smaller with *DaPe*, and is nearly overlapped when it is larger than 8. The conversion enhancement of CO_2 and CH_4 shown in Fig. 2 (d) embodies similar results to Fig. 2 (a) and (b). Taking the results shown in Fig. 2 together,

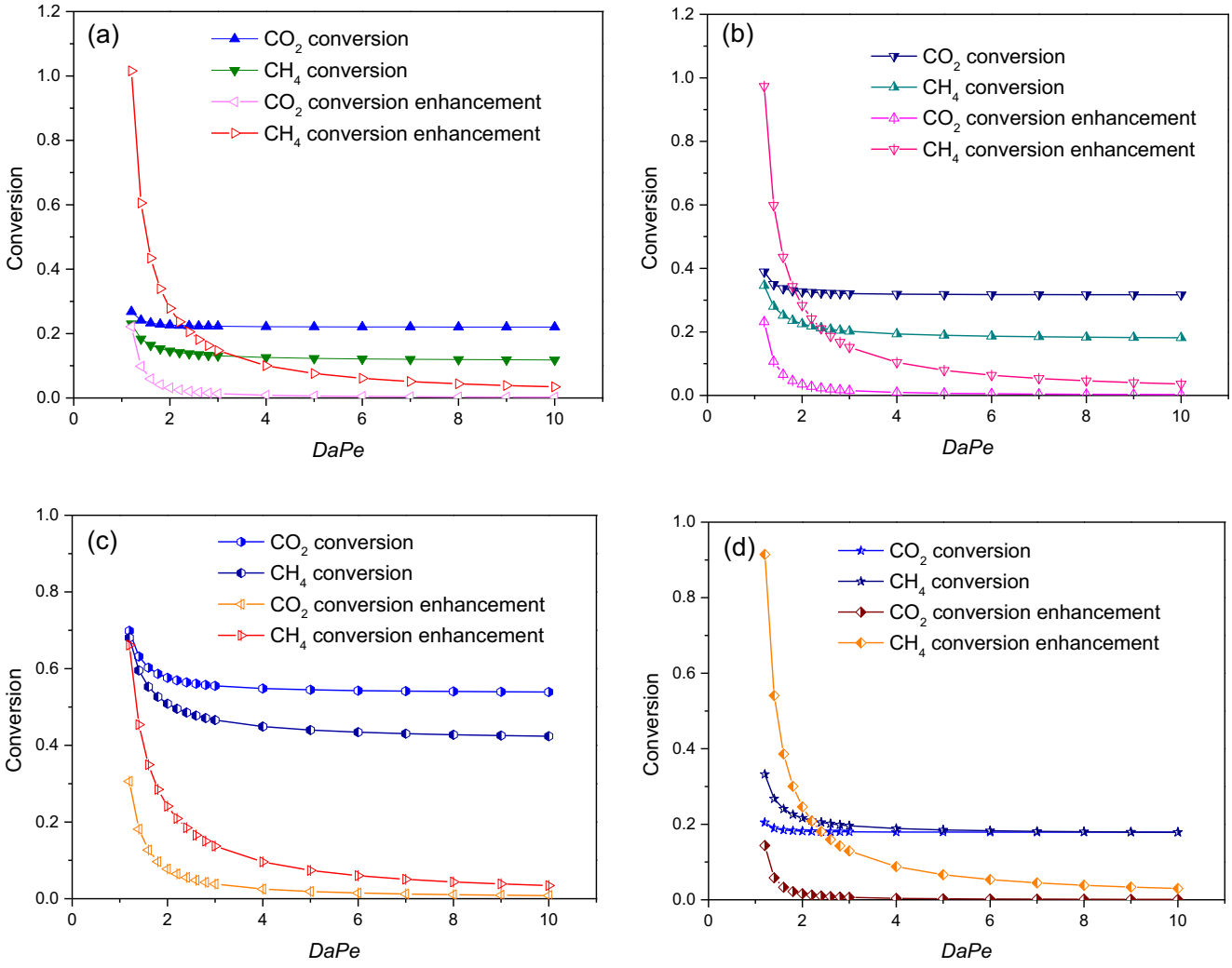

Fig. 2. CH_4 and CO_2 conversions of DRM and their enhancement in membrane reactors: (a) T = 600 ℃, p_t = 20 bar, and CH_4:CO_2 = 1:1; (b) T = 650 ℃, p_t = 20 bar, and CH_4:CO_2 = 1:1; (c) T = 600 ℃, p_t = 1 bar, and CH_4:CO_2 = 1:1; (d) T = 600 ℃, p_t = 20 bar and CH_4:CO_2 = 1:2.

another finding is that conversion enhancement is inversely proportional to conversion.

In the case of the independent RWGS, when the feed composition of H_2 and CO_2 is stoichiometric, i.e. H_2:CO_2 = 1:1, the conversions of H_2 and CO_2 are the same in Fig. 3 (a). Across the entire range of the *DaPe*, the conversions range from 73.8% to 54.8% and the corresponding conversion enhancement is from 37.9% to 2.4%. The critical value of the *DaPe* for achieving the "effective enhancement" is 1.7, which imposes a higher requirement for membrane permeation.

Increasing the H_2 molar fraction is an effective means of boosting the CO_2 conversion. When H_2:CO_2 = 3:1, the CO_2 conversion is three times that of H_2, as displayed in Fig. 3 (b). However, the conversion enhancement of H_2 and CO_2 remains the same (19.9% and 1.7%, respectively), but is much lower than the enhancement with stoichiometric feed composition. At a *DaPe* of 1.2, the CO_2 conversion approaches completion (94.5%), which is ready for downstream synthesis reactions, such as the Fischer-Tropsch synthesis. It is noticeable that the standard of "effective enhancement" cannot be met, even with the lowest *DaPe*.

The impacts of temperature on the conversions are not strong. Even when the temperature is reduced to 600 ℃, the conversions of H_2 and CO_2 range from 59.7% to 38.9% (Fig. 3 (c)). This is because the equilibrium constant is not sensitive to temperature, suggesting that increasing the temperature to achieve a high conversion is not optimal.

3. CFD simulations

In the above sections, we outlined the relationship of equilibrium constant-conversion-*DaPe*, and it was exemplified by the DRM and independent RWGS. Yet this relationship was derived from an equilibrium perspective, and there remain many aspects that cannot be reflected, including the compatibility of reaction kinetics with membrane permeation and the influence of the characteristics of reactor geometry. In this section, CFD simulations are performed for the same reactions from a kinetic perspective.

3.1. Model geometry

The model geometry of the membrane reactor is a tube-in-tube design of which the inner tube is for sweep gas and the outer tube for reacting gas. In our simulations, the reactor models are simplified as 2D axisymmetric models, as is shown in Fig. 4. The reacting and sweep gases are in counter-current flows in order to obtain a larger mean driving force for membrane permeation. The inner tube diameter is 7 mm, the outer one is 25 mm, and the length is 400 mm (Said et al., 2015).

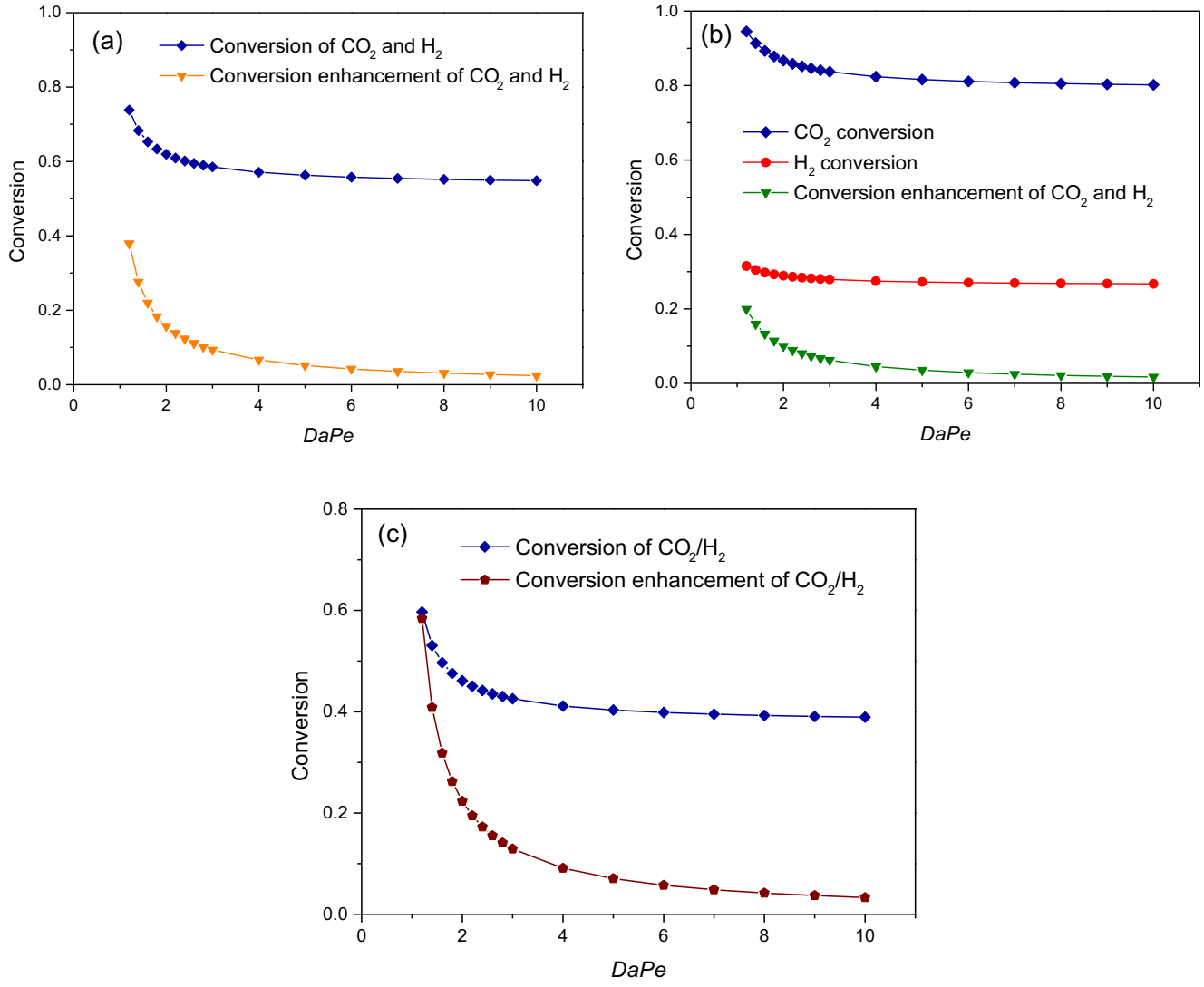

Fig. 3. H_2 and CO_2 conversions of RWGS and their enhancement in membrane reactors: (a) T = 900 ℃, p_t = 30 bar and H_2:CO_2 = 1:1; (b) T = 900 ℃, p_t = 30 bar and H_2:CO_2 = 3:1; (c) T = 600 ℃, p_t = 30 bar and H_2:CO_2 = 1:1.

3.2. Mass balance

The general form of mass conservation equation is expressed below, which is in a differential form (ANSYS Inc., 2016):

$$\frac{\partial \rho}{\partial t} + \frac{\partial}{\partial x}(\rho v_x) + \frac{\partial}{\partial r}(\rho v_r) + \frac{\rho v_r}{r} = S_m \tag{17}$$

where ρ is fluid density, x and r represent axial and radial coordinates, v_x and v_r are axial and radial velocities, and S_m is source term of mass. The above equation is applicable for incompressible and compressible flows.

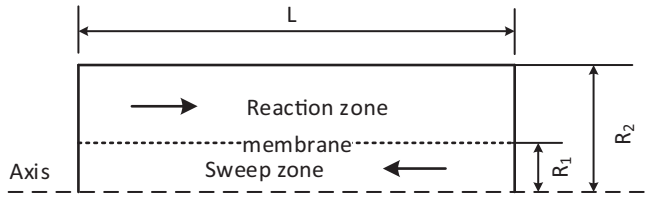

Fig. 4. Model geometry of the membrane reactor, R_1 = 7 mm, R_2 = 25 mm, and L = 400 mm.

If chemical reactions are involved in the system, the mass conservation equation is specifically written as follows (ANSYS Inc., 2016):

$$\frac{\partial}{\partial t}(\rho Y_i) + \frac{\partial}{\partial x}(\rho v_x Y_i) + \frac{\partial}{\partial r}(\rho v_r Y_i) + \frac{\rho v_r Y_i}{r} = -\left(\frac{\partial J_{i,x}}{\partial x} + \frac{\partial J_{i,r}}{\partial r} + \frac{J_{i,r}}{r}\right) + \eta_o r_i + S_i \tag{18}$$

$$J_i = -\sum_{j=1}^{N-1} \rho D_{ij} \nabla Y_j - D_{T,i} \frac{\nabla T}{T} \tag{19}$$

where Y_i is local mass fraction of each species, J_i is diffusion flux, and the D_{ij} and $D_{T,i}$ thereof are binary and thermal diffusion coefficients, respectively. r_i is reaction rate and η_o is the overall effectiveness factor that accounts for both external and internal mass transport limitations, and S_i is source term. Eq. (18) is a convection–diffusion equation, which consists of different terms that account for different mass transport mechanisms. The first term on the left side is unsteady mass flux, and the other three are mass fluxes by convection. The first term on the right side represents diffusive flux, and the second represents species generation or disap-

pearance via reactions; the last one is the membrane permeation, which is denoted by a source term. To solve the above equation, the species transport model is enabled with volumetric reaction selected in the ANSYS Fluent. Eq. (19) denotes diffusive mass fluxes by concentration and temperature gradients. Since the species transport in the radial direction of the membrane reactor is of particular importance, the full multicomponent diffusion option is enabled. The full multicomponent diffusion is suitable for diffusion-dominated laminar flows, which is based on the Maxwell-Stefan equation to calculate diffusive mass fluxes. The Maxwell-Stefan equation considers not only concentration gradients of species but also collisions between molecules, and therefore it is applicable for multicomponent systems. In addition, the temperatures of the reactor inlet and the wall are different, to account for the mass diffusion by the temperature gradient, the thermal diffusion option is also considered. Since the reaction rates are not in standard forms, they are calculated by user defined functions (UDFs) through the macro of DEFINE_VR_RATE. The modelling of membrane permeation processes are realized by the macros of DEFINE_ADJUST and DEFINE_SOURCE. The solution algorithm for pressure–velocity coupling is *coupled*, and the spatial discretization methods for species and energy are both *second order upwind* to get higher accuracy.

For the DRM, reliable kinetics over an Rh catalyst developed by Richardson (Richardson and Paripatyadar, 1990) is shown in Eqs. (20–27), which is presented in the classical LHHW form:

$$r_1 = \frac{k_1 K_{CO_2 1} K_{CH_4} p_{CO_2} p_{CH_4}}{\left(1 + K_{CO_2 1} p_{CO_2} + K_{CH_4} p_{CH_4}\right)^2} \left(1 - \frac{p_{CO}^2 p_{H_2}^2}{K_{eq1} p_{CO_2} p_{CH_4}}\right) \tag{20}$$

$$k_1 = 1290\exp(-102065/RT) \quad \text{mol}/(g_{cat}\ \text{s}) \tag{21}$$

$$K_{CO_2 1} = 0.0261\exp(37641/RT) \ \text{atm}^{-1} \tag{22}$$

$$K_{CH_4} = 0.026\exp(40684/RT) \ \text{atm}^{-1} \tag{23}$$

$$r_2 = \frac{k_2 K_{CO_2 2} K_{H_2} p_{CO_2} p_{H_2}}{\left(1 + K_{CO_2 2} p_{CO_2} + K_{H_2} p_{H_2}\right)^2} \left(1 - \frac{p_{CO} p_{H_2}}{K_{eq2} p_{CO_2} p_{H_2}}\right) \tag{24}$$

$$k_2 = 350\exp(-81030/RT) \quad \text{mol}/(g_{cat}\ \text{s}) \tag{25}$$

$$K_{CO_2 2} = 0.5771\exp(9262/RT) \quad \text{atm}^{-1} \tag{26}$$

$$K_{H_2} = 1.494\exp(6025/RT) \quad \text{atm}^{-1} \tag{27}$$

For the independent RWGS, Ni-based catalysts were found to be suitable and have been proven stable at a high temperature up to 900 ℃. A kinetics developed by (Wolf et al., 2016) is employed in simulations; as is shown in Eqs. (28–29). The reaction order with respect to H_2 is 0.3, suggesting the reaction rate is not very sensitive to H_2 concentrations.

$$r_3 = k_3 \left(c_{CO_2} c_{H_2}^{0.3} - \frac{c_{CO} c_{H_2O}}{K_{eq3} c_{H_2}^{0.7}}\right) \tag{28}$$

$$k_3 = 3100\exp(-82000/RT) \quad \text{mol kg}^{-1}\ \text{s}^{-1} \tag{29}$$

3.3. Membrane permeation modeling

Here, the membrane permeation process is abstracted as a source term, and is incorporated into the mass balance equation. The feed side is a negative source term and the sweep side a positive one. As the ANSYS Fluent solver is based on the finite volume method (FVM), it is necessary to convert the permeation flux from area-specific to volume-specific. The A_{cell} in Eq. (30) is the area of a single cell adjacent to the membrane wall and the V_{cell} is its corresponding volume. The membrane wall is heat coupled for conjugate heat transfer between the reaction zone and sweep gas zone.

$$S_i = \begin{cases} -\frac{J_i \cdot A_{cell}}{V_{cell}} & \text{Feed side} \\ +\frac{J_i \cdot A_{cell}}{V_{cell}} & \text{Sweep side} \end{cases} \tag{30}$$

A commercial palladium membrane was used for hydrogen permeation, and a zeolite membrane for water permeation. The permeation rates were calculated by the flux equations (Rohde et al., 2008); (Simakov and Sheintuch, 2011), as follows:

$$J_{H_2} = k_{H_2} \exp\left(\frac{-E_{H_2}}{RT}\right)\left(P_{H_2,f}^{0.5} - P_{H_2,s}^{0.5}\right) \tag{31}$$

$$J_{H_2O} = Q_{H_2O}\left(p_{H_2O,f} - p_{H_2O,s}\right) \tag{32}$$

where Q_{H_2O} is the permeance of water, 1E-6 mol/(m^2 s Pa), k_{H_2} = 1.26E-3 mol/(m^2 s Pa), E_{H_2} = 6.6 kJ/mol. The selectivities of the zeolite and palladium membranes are assumed to be infinite in our simulations, as their selectivities are usually very high (Rohde et al., 2008); (Yun and Ted Oyama, 2011).

3.4. Simulation results

All of the simulations were run for the DRM and RWGS in the range of 90 to 900 h^{-1} with respect to the gas hourly space velocity (GHSV). This range was determined according to the space time, from 40 to 4 s, which enables sufficient time for membrane permeation.

The reaction rates of the two reactions are presented by contours in Figs. 5 and 6. For the DRM, the maximum reaction rates of the DRM and RWGS are close, at 109 for the DRM and 121 mol/(m^3 s) for the RWGS, suggesting that the side-reaction plays a key role in regulating the selectivity and yield of H_2. For the independent RWGS, the maximum reaction rate is 899 mol/(m^3 s), which is much faster than that of the DRM. One feature that both reactions have in common is that the reactions are clustered in small regions close to the reactors' inlets, as indicated by the red color piece in the contours. At this point, the reactors' space is not sufficiently utilized, leading to a reduction in productivity. In principle, the reactor space should be made the best possible use of it, but this is constrained by membrane permeation fluxes. An implication here is that reaction rates should match the membrane permeation flux. However, current membrane permeation fluxes are typically on the order of 10^{-2} – 10^{-1} mol/(m^2 s) (Rahimpour et al., 2017). It can be imagined that reactions with lower reaction rates are more compatible with membranes, as the price of reduced productivity must not be paid. (van de Graaf et al., 1999) suggested use of the "window of reality" to judge if a reaction is compatible with membranes. It was shown that the space–time yield (STY) of a reaction should be located in the range of 1 – 10 mol/(m^3 s), such that it is compatible with the current membrane fluxes. Methanol synthesis from CO_2 and H_2 is one such reaction, with an STY of around 2 mol/(m^3 s), and space time as high as 25.2 s (Becka, 2018), which is already long enough for membrane permeation. Membrane reactors can be readily used for this reaction. With the improvements in the membrane flux, the boundary of the "window of reality" will be expanded, so that reactions with fast kinetics with low equilibrium conversions can be included.

The species molar fractions are depicted in Figs. 7 and 8. For both reactions, with a low GHSV of 90 h^{-1}, the H_2/H_2O mole fractions increase to the maximum in the vicinity of the reactor inlets,

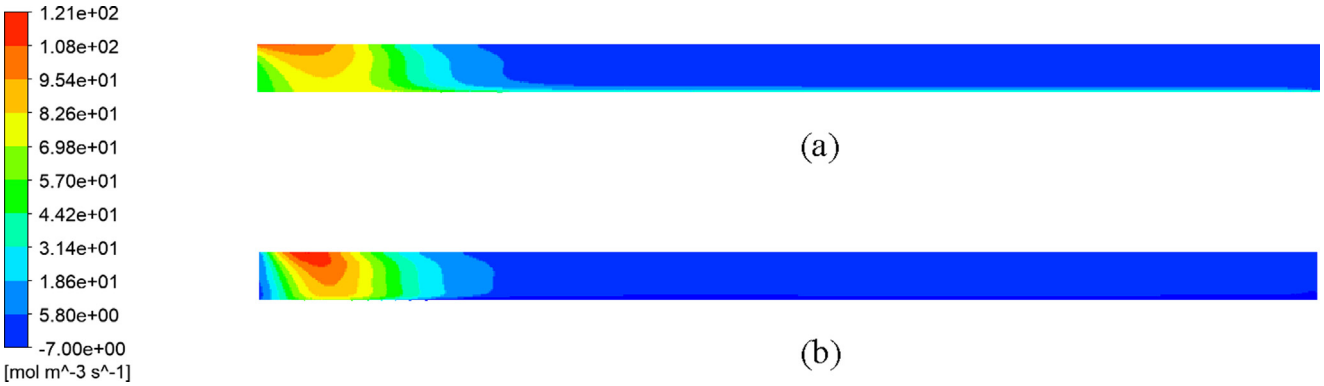

Fig. 5. Reaction kinetics of the (a) DRM; (b) RWGS, T = 600 ℃, p_t = 20 bar, CH_4:CO_2 = 1:1, and GHSV = 900 h^{-1}.

Fig. 6. Reaction kinetics of the independent RWGS, T = 900 ℃, p_t = 30 bar, H_2:CO_2 = 1:1, and GHSV = 900 h^{-1}.

indicating that reactions have reached equilibria. At higher GHSV of 900 h^{-1}, the distance needed to reach the maximum molar fractions becomes longer. At GHSV of 90 h^{-1}, it is also observed that thick boundary layers are formed alongside the membrane surfaces, and the concentration gradient is obvious. Two reasons underpin the formation of the boundary layers: first, at a GHSV = 90 h^{-1}, the percentage of species removal is high, leading to the deficit of species surrounding the membranes; second, the flow is laminar across the entire range of the GHSV (Reynolds number Re < 2300), and the mass transport by forced convection is slow, especially within the boundary layers. Instead, molecular diffusion is the primary mass transport mechanism in the radial direction, despite which the concentration gradient can trigger natural convection. The presence of the concentration gradient suggests that mass transport in the radial direction falls behind the membrane fluxes. The concentration gradient can, in some cases, lead to a decline in conversion by around 50%, as was pointed out by (Godini et al., 2014). The concentration gradient can be alleviated in different respects; including: (1) The intensification of mass transport in the radial direction. Placing spacers in membrane reactors to increase turbulence is an effective approach; using fluidized bed reactors is also helpful for radial mixing so that concentration distribution is more even. (2) Optimization of the geometric characteristics. The geometric characteristics can be reflected using the ratio of the membrane area to reactor volume $A/V = 2r_1/(r_2^2 - r_1^2)$. The A/V has the important feature that it only contains the radius and is irrelevant to the reactor's length. In principle, a larger A/V is preferred, as the mass transport distance is shorter. A larger A/V can be achieved by either reducing r_2 or increasing r_1, or doing both simultaneously. In a study by (van de Graaf et al., 1999); the A/V was suggested to be in the range of 10 – 100 m^{-1}. In our models, the A/V is equal to 24.3, which is smaller than the medium value, suggesting some space for improvement.

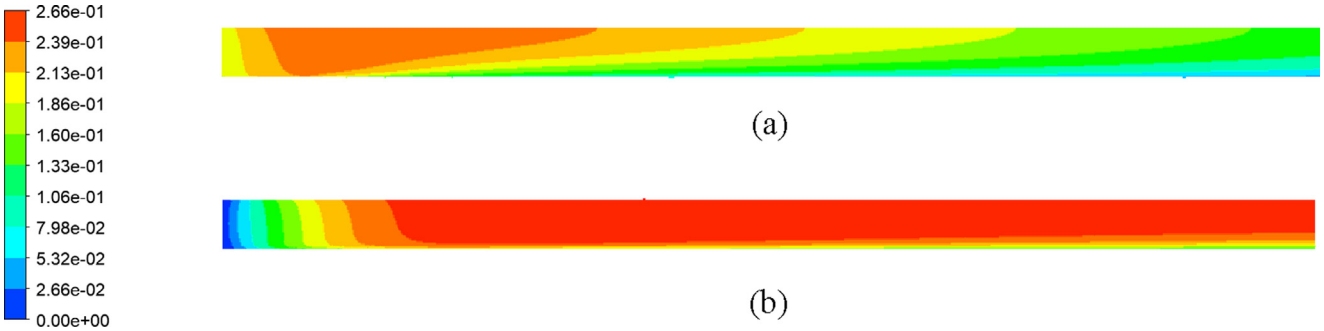

Fig. 7. Molar fraction of H_2 of the DRM: (a) GHSV = 90 h^{-1}, and (b) GHSV = 900 h^{-1}.

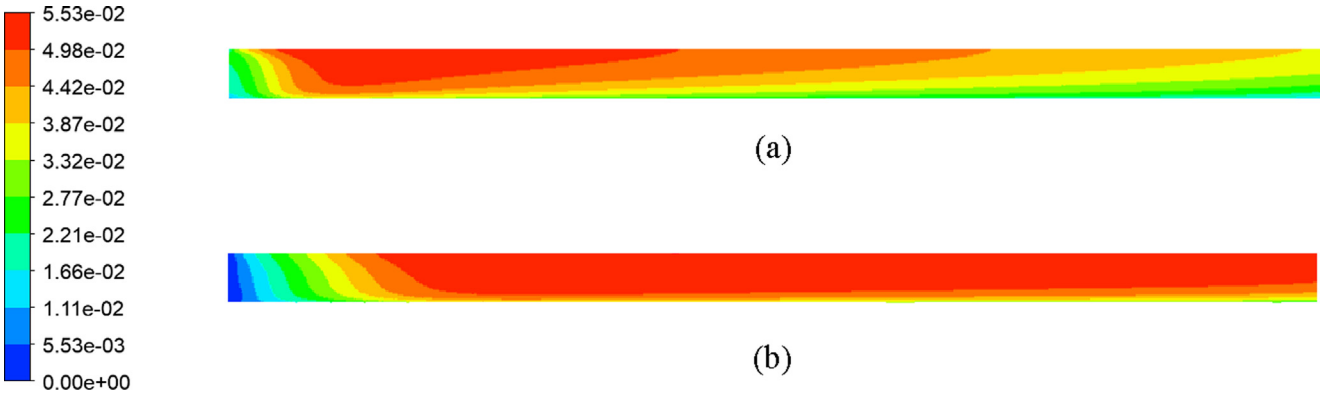

Fig. 8. Molar fraction of H_2O of the independent RWGS: (a) GHSV = 90 h^{-1}; and (b) GHSV = 900 h^{-1}.

3.5. Comparison with theoretical calculations

In order to consolidate the conclusions obtained from the theoretical calculations, Fig. 9 shows conversions via CFD simulations and comparisons with theoretical calculations. The conversions of the two reactions are compared under different operating conditions. The results from the CFD simulations agree well with the theoretical calculations, and the relationship is, as such, validated.

4. Discussion

The sections above exemplified the relationship of the equilibrium constant-conversion-*DaPe* by applying it to the DRM and the independent RWGS, which is validated by CFD simulations. However, a comparison has not yet been made between the two reactions. To find differences between them and what accounts for these, here we collapse the results onto a single figure in terms of conversion enhancement. To make a fair comparison, Fig. 10 is generated under the same operating conditions in order to identify the contributions by membranes alone .

In the above figure, the conversion enhancement of the DRM is always higher than that of the independent RWGS, regardless of what the *DaPe* is. Two factors account for this: although the operating temperatures are kept the same, this does not ensure the same equilibrium constants, of 0.197 for the DRM and 0.366 for the RWGS. The equilibrium constant K_{eq} can be used as a proxy for conversion, as conversion is a strictly increasing, sigmoidal function of K_{eq} that ranges from 0 to 1 (Schiffer et al., 2021). As we conclude above, conversion enhancement and the conversion of a reaction are inversely proportional, which means that any

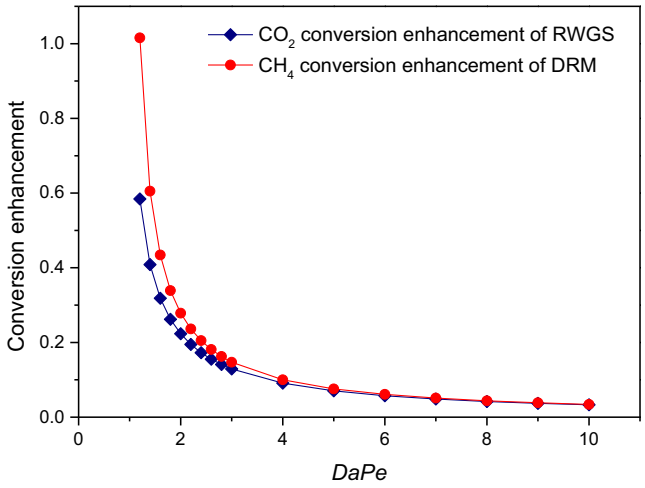

Fig. 10. Comparison of conversion enhancement of the DRM and the independent RWGS under the same operating conditions, T = 600 ℃, p_t = 30 bar, and the stoichiometric feed composition.

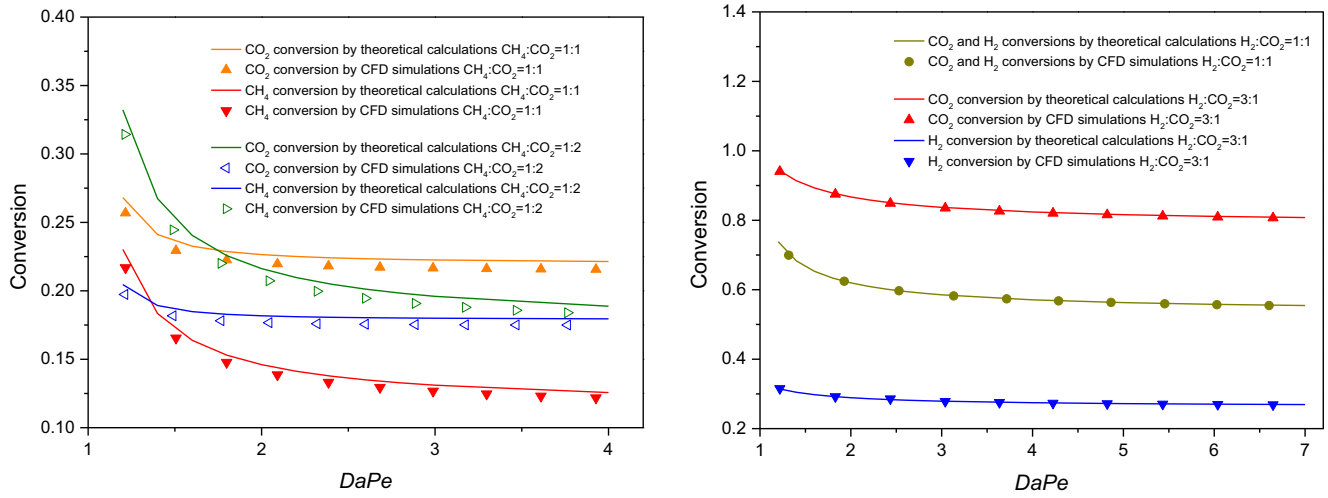

Fig. 9. Comparison of conversions by theoretical calculations and CFD simulations: (a) DRM, T = 600 ℃, p_t = 20 bar; and (b) independent RWGS, T = 900 ℃, p_t = 30 bar.

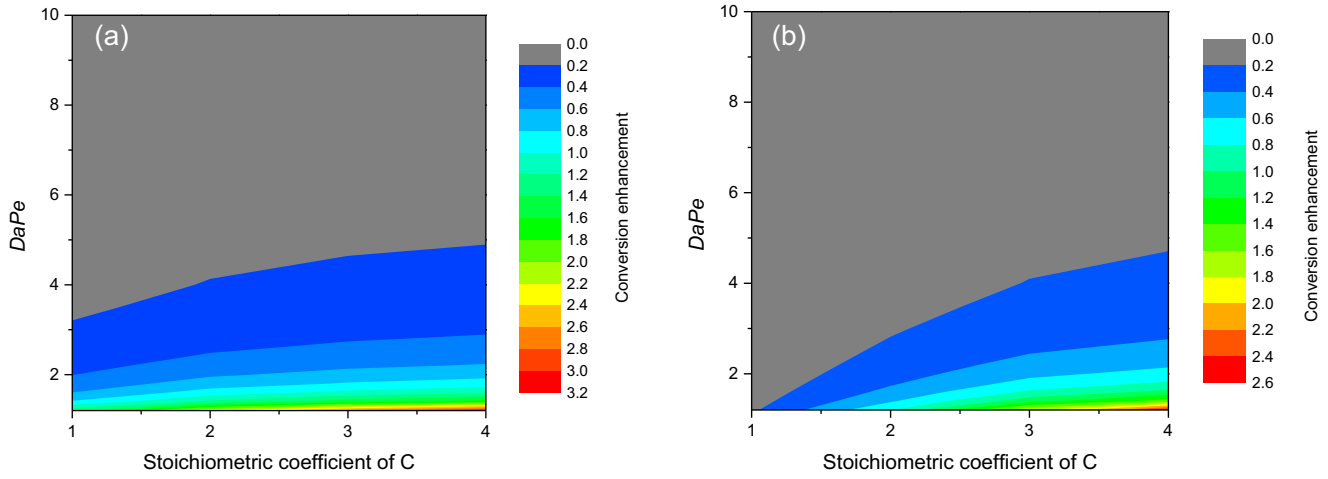

Fig. 11. *DaPe*-stoichiometric coefficient plot for the conversion enhancement analysis at different equilibrium constants: (a) K_{eq} = 10^{-3}; and (b) K_{eq} = 10. C is the product to be removed by membranes.

factor that leads to a higher equilibrium constant will reduce the conversion enhancement. Thus, the conversion enhancement of the independent RWGS is lower. Another important factor is the stoichiometric coefficient of the product to be removed. In Eq. (2), K_{eq} is expressed as the quotient of the partial pressure exponents of products and reactants, with the pressure exponents corresponding to the stoichiometric coefficients of each species. The stoichiometric coefficient with respect to the H_2 of the DRM is two, whereas the stoichiometric coefficient with respect to H_2O of the independent RWGS is one. A higher stoichiometric coefficient has a stronger impact on conversion enhancement with the same *DaPe* value.

Stoichiometric coefficients reflect a structural difference across different reactions. Thus far, our analysis of the effects of the stoichiometric coefficient has focused on the two specific reactions. Next, we want to see if this is applicable for general cases. To do this, we must separately observe the effects of the stoichiometric coefficient in a general form. As there are many other factors that affect the enhancement, we employ the variable-controlling method by fixing other variables, while only adjusting the stoichiometric coefficient of the product to be removed. For the sake of simplicity, the stoichiometric coefficients of A, B, and D are unity, whereas that of C is adjustable in Eq. (1).

The effect of the stoichiometric coefficient on conversion is implicit, and therefore we provide a facile visualization for intuitive quantification and comparison purposes, shown in Fig. 11. Each plot below was generated with different combinations of *DaPe* and stoichiometric coefficient. The left figure is for K_{eq} = 10^{-3}, and represents highly limited reactions, whereas the right one is for reactions with a moderate K_{eq} = 10. In both figures, for a particular *DaPe*, higher conversion enhancement is always obtained for larger stoichiometric coefficients. The higher the stoichiometric coefficient is, the larger the conversion enhancement could be. In other words, in order to achieve the same conversion enhancement, higher stoichiometric coefficients allow larger *DaPe* values. The highest conversion enhancement is obtained at the highest stoichiometric coefficient combined with the lowest *DaPe* (lower right corner). The maximum conversion enhancement of the left figure is 320%, whereas that of the right figure is 260%, which once again confirms the conclusion that the conversion and its enhancement are inversely proportional.

The discrimination of feasible and infeasible regimes by the 20% threshold value of "effective enhancement" is also displayed, with the infeasible regimes highlighted by the gray color. For reactions with very low K_{eq} of 10^{-3}, the gray area is smaller, suggesting that membrane reactors contribute more effectively to highly limited reactions. For reactions with a moderate K_{eq} of 10, the infeasible regime is larger, especially for a stoichiometric coefficient of one, the standard of "effective enhancement" cannot be met, even with the lowest *DaPe*. In such circumstances, leveraging the contribution of the stoichiometric coefficient is an effective way to gain larger conversion enhancement, by which the critical role of the stoichiometric coefficient is highlighted.

5. Conclusions

Membrane reactors are widely used for chemical reactions, yet most of the previous studies on membrane selection and matching are often simply based on qualitative analysis and judgement in a case-by-case manner. To address the question of how to select and match suitable membranes for a reaction, this study was conducted in a general and quantified form from the following three aspects.

First, the relationship of the equilibrium constant-conversion-*DaPe* was built by introducing the Damköhler and Péclet numbers. The relationship includes the parameters of the operating condition and reaction stoichiometric coefficient, which is universally applicable for membrane reactor concepts with single product removal. For the purpose of validation, the relationship was then applied to the reactions of the dry reforming of methane and reverse water gas shift by theoretical calculations.

Second, CFD simulations were performed to analyze compatibility from the perspectives of the reaction kinetics-permeation flux and reactor geometric characteristics. The operating window of reaction kinetics and the membrane permeation flux have been identified and suitable surface to volume ratios of membrane reactors analyzed.

Finally, the contribution of the stoichiometric coefficient to conversion enhancement has been identified and highlighted, with the finding that the larger the stoichiometric coefficient is, the higher the conversion enhancement could be under the same operating conditions. The role of the stoichiometric coefficient is important for deciding which component is to be removed to obtain higher conversion enhancement.

As the varieties of membranes continue to increase, the need for the guidance for the selection and matching of membranes for a given reaction will become ever more urgent. The relationships

derived in this study could help shift membrane reactor selection and matching from relying on heuristics to dependence on quantified analysis.

CRediT authorship contribution statement

Hong Huang: Conceptualization, Methodology, Software, Validation, Formal analysis, Writing – original draft. **Remzi Can Samsun:** Writing – review & editing. **Ralf Peters:** Writing – review & editing. **Detlef Stolten:** Supervision.

Declaration of Competing Interest

The authors declare that they have no known competing financial interests or personal relationships that could have appeared to influence the work reported in this paper.

Acknowledgments

The authors would like to thank the Guangzhou Elite Project (JY201801) for the scholarship supporting the PhD project of Hong Huang.

References

Al-Megren, H.A., Barbieri, G., Mirabelli, I., Brunetti, A., Drioli, E., Al-Kinany, M.C., 2013. Direct Conversion of n-Butane to Isobutene in a Membrane Reactor: Thermodynamic Analysis. Industrial & Engineering Chemistry Research 52 (31), 10380–10386.

ANSYS Inc., 2016. ANSYS Fluent Theory Guide 17.2.

Barbieri, Giuseppe, Marigliano, Giuseppe, Golemme, Giovanni, Drioli, Enrico, 2002. Simulation of CO2 hydrogenation with CH3OH removal in a zeolite membrane reactor. Chemical Engineering Journal 85 (1), 53–59.

Becka, R., 2018. CFD-Modelling and Evaluation of Methanol Synthesis Reactors for Power-to-Fuel Application Master Thesis. RWTH Aachen University.

Bernstein, L.A., Lund, C.R.F., 1993. Membrane reactors for catalytic series and series-parallel reactions. Journal of Membrane Science 77 (2-3), 155–164.

Dixon, Anthony G, 2001. Analysis of intermediate product yield in distributed-feed nonisothermal tubular membrane reactors. Catalysis Today 67 (1-3), 189–203.

Fabián-Anguiano, J.A., Mendoza-Serrato, C.G., Gómez-Yáñez, C., Zeifert, B., Ma, Xiaoli, Ortiz-Landeros, J., 2019. Simultaneous CO2 and O2 separation coupled to oxy-dry reforming of CH4 by means of a ceramic-carbonate membrane reactor for in situ syngas production. Chemical Engineering Science 210, 115250. https://doi.org/10.1016/j.ces.2019.115250.

Gallucci, F., Basile, A., 2007. A theoretical analysis of methanol synthesis from CO2 and H2 in a ceramic membrane reactor. International Journal of Hydrogen Energy 32 (18), 5050–5058.

Gallucci, Fausto, Paturzo, Luca, Basile, Angelo, 2004. An experimental study of CO2 hydrogenation into methanol involving a zeolite membrane reactor. Chemical Engineering and Processing: Process Intensification 43 (8), 1029–1036.

Godini, H.R., Xiao, S., Kim, M., Holst, N., Jašo, S., Görke, O., Steinbach, J., Wozny, G., 2014. Experimental and model-based analysis of membrane reactor performance for methane oxidative coupling: Effect of radial heat and mass transfer. Journal of Industrial and Engineering Chemistry 20 (4), 1993–2002.

Iulianelli, A., Manzolini, G., De Falco, M., Campanari, S., Longo, T., Liguori, S., Basile, A., 2010. H2 production by low pressure methane steam reforming in a Pd–Ag membrane reactor over a Ni-based catalyst: Experimental and modeling. International Journal of Hydrogen Energy 35 (20), 11514–11524.

Kim, Sehwa, Ryi, Shin-Kun, Lim, Hankwon, 2018. Techno-economic analysis (TEA) for CO2 reforming of methane in a membrane reactor for simultaneous CO2 utilization and ultra-pure H2 production. International Journal of Hydrogen Energy 43 (11), 5881–5893.

Kim, Sehwa, Yun, Su-Won, Lee, Boreum, Heo, Juheon, Kim, Kihyung, Kim, Yong-Tae, Lim, Hankwon, 2019. Steam reforming of methanol for ultra-pure H2 production in a membrane reactor: Techno-economic analysis. International Journal of Hydrogen Energy 44 (4), 2330–2339.

Moon, W.S., Park, S.B., 2000. Design guide of a membrane for a membrane reactor in terms of permeability and selectivity. Journal of Membrane Science 170, 43–51.

Oyama, S. Ted, Lim, Hankwon, 2009. An operability level coefficient (OLC) as a useful tool for correlating the performance of membrane reactors. Chemical Engineering Journal 151 (1-3), 351–358.

Patrascu, Michael, Sheintuch, Moshe, 2015. On-site pure hydrogen production by methane steam reforming in high flux membrane reactor: Experimental validation, model predictions and membrane inhibition. Chemical Engineering Journal 262, 862–874.

Rahimpour, M.R., Samimi, F., Babapoor, A., Tohidian, T., Mohebi, S., 2017. Palladium membranes applications in reaction systems for hydrogen separation and purification: A review. Chemical Engineering and Processing: Process Intensification 121, 24–49.

Raso, R., Tovar, M., Lasobras, J., Herguido, J., Kumakiri, I., Araki, S., Menéndez, M., 2021. Zeolite membranes: Comparison in the separation of H2O/H2/CO2 mixtures and test of a reactor for CO2 hydrogenation to methanol. Catalysis Today 364, 270–275.

Rezai, S., Traa, Y., 2008. Equilibrium shift in membrane reactors: A thermodynamic analysis of the dehydrogenative conversion of alkanes. Journal of Membrane Science 319 (1-2), 279–285.

Richardson, J.T., Paripatyadar, S.A., 1990. Carbon dioxide reforming of methane with supported rhodium. Applied Catalysis 61 (1), 293–309.

Rohde, M.P., Schaub, G., Khajavi, S., Jansen, J.C., Kapteijn, F., 2008. Fischer-Tropsch synthesis with in situ H2O removal – Directions of membrane development. Microporous and Mesoporous Materials 115 (1-2), 123–136.

Said, Syed A.M., Simakov, David S.A., Mokheimer, Esmail M.A., Habib, Mohamed A., Ahmed, Shakeel, Waseeuddin, Mohammed, Román-Leshkov, Yuriy, 2015. Computational fluid dynamics study of hydrogen generation by low temperature methane reforming in a membrane reactor. International Journal of Hydrogen Energy 40 (8), 3158–3169.

Schiffer, Zachary J., Limaye, Aditya M., Manthiram, Karthish, 2021. Thermodynamic Discrimination between Energy Sources for Chemical Reactions. Joule 5 (1), 135–148.

Simakov, David S.A., Sheintuch, Moshe, 2011. Model-based optimization of hydrogen generation by methane steam reforming in autothermal packed-bed membrane reformer. AIChE Journal 57 (2), 525–541.

Sommer, David E., Kirchen, Patrick, 2019. Towards improved partial oxidation product yield in mixed ionic-electronic membrane reactors using CSTR and CFD modelling. Chemical Engineering Science 195, 11–22.

van de Graaf, Jolinde M., Zwiep, Marco, Kapteijn, Freek, Moulijn, Jacob A., 1999. Application of a silicalite-1 membrane reactor in metathesis reactions. Applied Catalysis A: General 178 (2), 225–241.

Wade, Jennifer L., Lee, Catherine, West, Alan C., Lackner, Klaus S., 2011. Composite electrolyte membranes for high temperature CO2 separation. Journal of Membrane Science 369 (1-2), 20–29.

Wolf, Andreas, Jess, Andreas, Kern, Christoph, 2016. Syngas Production via Reverse Water-Gas Shift Reaction over a Ni-Al2O3 Catalyst: Catalyst Stability, Reaction Kinetics, and Modeling. Chemical Engineering & Technology 39 (6), 1040–1048.

Wu, Han-Chun, Rui, Zebao, Lin, Jerry Y.S., 2020. Hydrogen production with carbon dioxide capture by dual-phase ceramic-carbonate membrane reactor via steam reforming of methane. Journal of Membrane Science 598, 117780. https://doi.org/10.1016/j.memsci.2019.117780.

Yang, Xuesong, Wang, Shuai, Hu, Bang, Zhang, Kai, He, Yurong, 2019. Estimation of concentration polarization in a fluidized bed reactor with Pd-based membranes via CFD approach. Journal of Membrane Science 581, 262–269.

Yun, Samhun, Ted Oyama, S., 2011. Correlations in palladium membranes for hydrogen separation: A review. Journal of Membrane Science 375 (1-2), 28–45.